Progress in Organic Coatings 103 (2017) 48–59

Contents lists available at ScienceDirect

Progress in Organic Coatings

journal homepage: www.elsevier.com/locate/porgcoat

Highly icephobic properties on slippery surfaces formed from polysiloxane and fluorinated POSS

Chao Tao [a], Xiaohui Li [a], Bo Liu [a], Kaiqiang Zhang [a], Yunhui Zhao [a], Kongying Zhu [b], Xiaoyan Yuan [a,*]

[a] School of Materials Science and Engineering, Tianjin Key Laboratory of Composite and Functional Materials, Tianjin University, Tianjin 300072, China
[b] Analysis and Measurement Center, Tianjin University, Tianjin 300072, China

ARTICLE INFO

Article history:
Received 7 June 2016
Received in revised form 25 October 2016
Accepted 5 November 2016

Keywords:
Fluorinated POSS
Polysiloxane
Slippery surface
Wavy surface
Icephobicity

ABSTRACT

Recent emerging strategies to prepare icephobic coatings have focused on slippery surfaces containing a liquid lubricant with low surface energy, which significantly reduces ice adhesion. In this work, a facile technique was developed for preparation of polysiloxane coatings with efficient and durable icephobicity. Fluorinated polyhedral oligomeric silsesquioxanes (F-POSS-SiH) with different fluorinated groups and Si-H active sites were synthesized via hydrosilylation between fluorinated methacrylates and octakis(dimethylsiloxy) octasilsequioxane. The F-POSS-SiH hybrid compound was subsequently applied as a co-crosslinker in the system of polymethylhydrosiloxane (PMHS) and polymethylvinylsiloxane to create silicone coatings. The low surface energy of fluorinated groups could drive F-POSS-SiH towards the coating surface, leading to a gradient distribution in which F-POSS-SiH was self-assembled on the top surface, while silicone was rich in the bottom layer. Meanwhile, wavy surfaces were generated spontaneously by compressive stress during the coating formation. The wavy microstructure of coatings provided space for the unreacted silicone oil, i.e., low molecular weight PMHS, that could be considered as a liquid lubricant and controlled by the dosage. Therefore, the slippery wavy coatings showed highly icephobic properties with extraordinarily low ice shear strengths at a lowest value of 3.8 ± 1.8 kPa, only 5 percentage of Sylgard 184. Moreover, the coatings remained icephobicity after 15 icing/deicing cycles, demonstrating excellent durability.

1. Introduction

Ice and frost accumulated on electric grids, aircrafts, wind turbine blades and other facility surfaces can cause severe destruction and massive casualties [1,2]. This issue can be prone to resolve by either delaying ice formation or reducing ice adhesion strength on the surface. Moreover, weakening the ice adhesion by icephobic coatings is preferable for it is difficult to prevent ice formation for a long time under subzero temperatures and high humidity conditions [3–5].

Over the past decades, efforts seemingly focused on superhydrophobic surfaces, which can inhibit impacting and condensed water drops before ice formation [6–10]. It has been reported that superhydrophobic surfaces displayed a robust icing-delay performance with a delay time of approximate 750 s at −10 °C [11]. Nevertheless, once ice accreted on a superhydrophobic surface, the icephobic property would be partially or completely destroyed owing to water drops penetrating into surface textures, which would cause interlocking effect between ice and the surface [3,12–14].

Aizenberg et al. proposed the concept of SLIPS (slippery liquid infused porous surface) by imitating nepenthes, and a molecular level slippery surface was obtained by infusing fluorinated fluids into porous surfaces [15]. Recently, textured surfaces with oily or aqueous lubricating layers have been created, providing extremely low ice adhesion and slippery characteristics [16–24]. However, the limited amount of bound water remains a challenge for aqueous lubricating coatings, since accumulation of excessive free water will accelerate icing. Hence, it would be prospective to construct slippery surfaces with a stable and continuously oil-replenishable lubricant layer. Wang et al. addressed silicone-oil-infused polydimethylsiloxane (PDMS) coatings with different silicone oil amounts and the substrate-lubricant-water/ice interface enabled probable removal of water drops or ice by natural force

* Corresponding author.
E-mail addresses: yuanxy@tju.edu.cn, xyuan28@yahoo.com (X. Yuan).

http://dx.doi.org/10.1016/j.porgcoat.2016.11.018
0300-9440/

[24]. Furthermore, it was mentioned that ice nuclei will more easily form on a solid surface than on the lubricant [25]. Textured or porous surfaces are conceived to accommodate or lock the lubricant in case the lubricant will be drained off quickly during deicing process. Although various methods have been employed to produce surface topographies, manipulations like photolithographic or mechanical micromachining require expensive equipment and multiple time-consuming processes [26].

Researches have specifically attempted to investigate the polymers brush as tethered lubricant [27] and the dewetting behavior of liquids on PDMS brush surfaces [28]. Wang et al. fabricated "omniphobic" surfaces based on acid catalyzed hydrolysis and step-growth graft polymerization of dimethyldimethoxysilane [29]. PDMS ($T_g = -127\,^{\circ}C$) was commonly used to produce polymer brushes since it is one of a few linear polymers to be considered a liquid at low temperatures even with high molecular weights. The polymer itself can also remain stable at temperatures over 200 °C. The above results offer clear evidence that PDMS, whose molecular chains still stay flexible at extremely low temperatures, is an appropriate material for lubricant and anti-icing coatings [24,25,30].

Inspired by micro/nano-structured natural plant surfaces, researchers have investigated the effect of surface morphology on wettability and icephobicity [31–33]. Chen et al. reported a hierarchical micro/nano-structured superhydrophobic surface that not only significantly suppressed the ice nucleation and inter-droplet freezing propagation during the frosting process, but also promoted fast frost removal at defrosting stage [34]. Surface wrinkles were of significant potential in film metrology and surface topology by introducing mico/nano-sized structures [26,35–37]. For instance, regular wrinkle patterns were generated by initiated chemical vapor deposition of poly(ethylene glycol diacrylate) film on biaxial pre-stretched PDMS substrate [35]. Jiang et al. prepared a photocuring coating with micro/nanowrinkling morphology by a polyhedral oligomeric silsesquioxane (POSS) with thiol and fluorocarbon groups as a reactive nanoadditive [36]. The tunable wrinkling features controlled by thickness and external force made them suitable candidates for actual applications. For example, it could be a facile and promising strategy to produce wrinkle-like surfaces for anti-icing.

Fluorinated materials have been widely used in hydrophobic or oleophobic modifications as well as icephobic purposes due to its low surface energy [38–40]. POSS is a kind of organic-inorganic hybrid molecules with an inorganic core surrounded by organic groups at eight corners [41,42]. Low surface energy, reactive and nanosized organic-inorganic hybrid molecules could be obtained by chemically combining fluoro-containing reactants with POSS [41].

In our previous publications, icephobic coatings have been developed from fluorosilicone methacrylate-polysiloxane block polymers synthesized via macro-azo-initiators or reversible addition-fragmentation chain transfer polymerization [43–46]. Submicron/nano-structured icephobic surfaces were also ever prepared from fluorinated polymethylsiloxane and octavinyl POSS [47]. Based on the low surface energy and low adhesion with ice of PDMS, POSS and fluorinated polymers, in this study, we attempted to develop a highly efficient and durable icephobic coating from polymethylvinylsiloxane (PMVS) and polymethylhydrosiloxane (PMHS) by introducing fluorinated POSS with SiH groups as a co-crosslinker. In order to obtain extraordinary low ice shear strength, fluorinated POSS were introduced even though it is not easy to prepare and has a higher price. It was suggested that excess PMHS controlled by the dosage could be encompassed as a lubricant in the slippery hybrid coatings with rough wavy surfaces generated by self-assembly of fluorinated POSS. Meanwhile, these icephobic coatings demonstrated icephobic durability after 15 icing/deicing cycles.

2. Experimental methods

2.1. Synthesis of fluorinated POSS

As shown in Scheme 1, three kinds of fluorinated POSS (F-POSS-SiH) were synthesized via hydrosilylation between octakis(dimethylsiloxy)-octasilsequioxane (OS-POSS) and fluorinated methacrylates (FMA), i.e., hexafluorobutyl methacrylate (6FMA), dodecafluoroheptyl methacrylate (12FMA) and tridecafluorooctyl methacrylate (13FMA), respectively. Take the synthesis of 6F-POSS-SiH for example, OS-POSS (0.50 g, 0.49 mol, Hybrid Plastics, USA) and 6FMA (0.49 g, 1.96 mol, ≥96%, XEOGIA, China) were mixed in toluene (2.31 g, Kemiou Chemical Reagent Co., Tianjin, China) in a three-neck flask fitted with a condenser and N_2 inlet under stirring, in which the molar content of reactive Si-H groups was ensured as twice as that of C=C bonds, i.e., FMA. Then, Karstedts' catalyst (0.1 mol% of Si—H bond) was added dropwise. The solution was allowed to stir at 80 °C for 48 h, followed by reduced pressure distillation and vacuum drying to remove unreacted monomer and toluene, and obtain a viscous resultant product. The synthesis process of 12F-POSS-SiH and 13F-POSS-SiH was the same as above.

Characterizations of 6F-POSS-SiH, 12F-POSS-SiH and 13F-POSS-SiH by Fourier transform infrared (FTIR, Perkin-Elmer Spectrum 100) and proton-nuclear magnetic resonance (^{1}H NMR, Varian INOVA at 500 MHz) were shown in Figs. 1 and 2 and the Supplementary data, respectively.

2.2. Preparation of hybrid polysiloxane coatings

Take the preparation of coatings comprising 6F-POSS-SiH for example, the prepared 6F-POSS-SiH (0.1 g) was mixed with PMHS (0.35 g, industrial grade, Hito Chemical Co., Jiangxi, China, $\overline{M} \approx 2000$ g/mol) and PMVS (0.55 g, industrial grade, Dayi Co., Shandong, China, $\overline{M} \approx 30000$ g/mol) in α,α,α-trifluorotoluene (TFT) (4.88 g, Kemiou Chemical Reagent Co., Tianjin, China). Afterwards, Karstedts' catalyst (0.1 mol% of Si-H bond) was added dropwise. The solution was placed on a turbine mixer (MS3, IKA, Germany) and stirred mechanically for 1 h. The coating was prepared by casting the solution (350 μL) on a 2 cm × 2 cm aluminium sheet, left at ambient temperature for 1 h and cured at 100 °C for 3 h in an air-circulating oven. The thickness of the coating was controlled by the solution volume on the aluminium sheet. The preparation of other series was the same as above. Compositions of the reactants used in the crosslinking system were shown in Table 1. Samples were named as **P*x*F*y*** which refered to the weight percentage (***x***) of F-POSS-SiH in the hybrid coatings and the fluorine number (***y***) of FMA used for preparation of the fluorinated POSS. Sample **P0** without F-POSS-SiH was prepared only from PMHS and PMVS as a control to examine the effect of F-POSS-H.

2.3. Characterizations

Scanning electron microscope (SEM) observation (s-4800, Hitachi Limited, Japan) equipped with electronic differential system (EDS) was carried out to analyze the surface morphology and the element distribution in the cross-section of the coatings. The coating on an aluminum sheet was glued to a sample stage by using conductive adhesive and sputtered with gold before SEM observation. Optical microscope (OM) images were obtained with an Olympus CKX41 microscope.

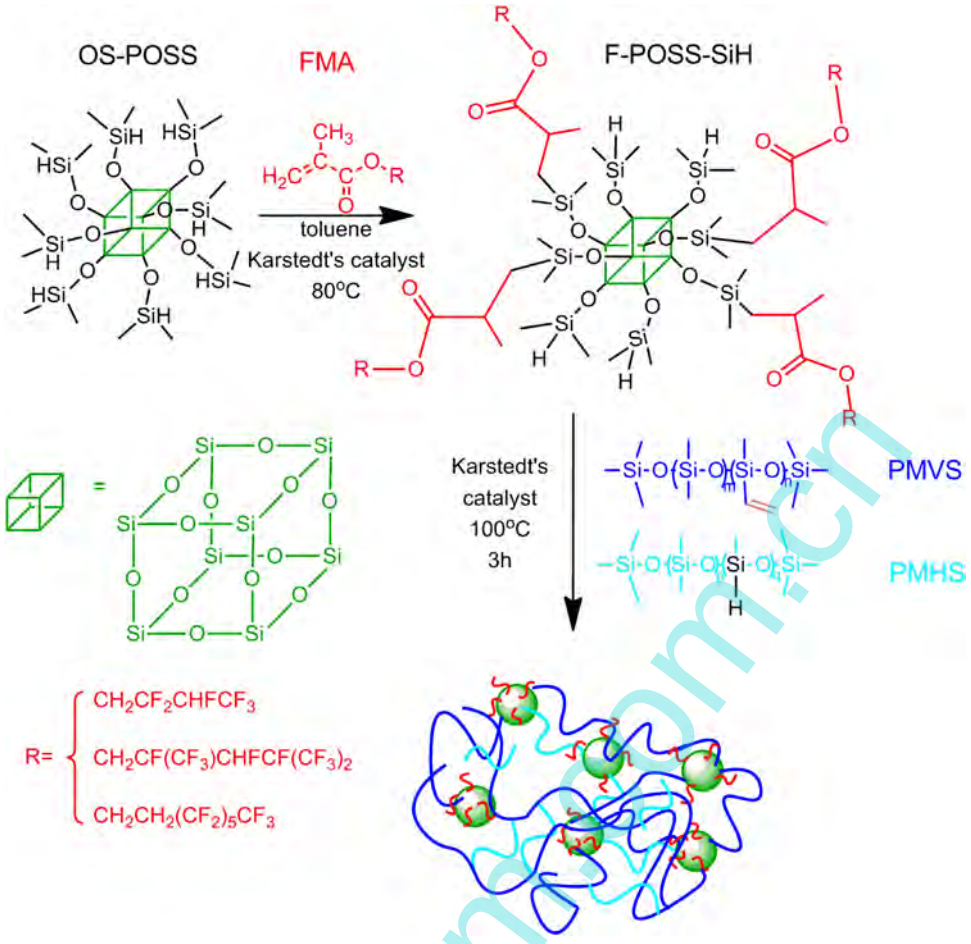

Scheme 1. Preparation of fluorinated POSS (6F-POSS-SiH, 12F-POSS-SiH, and 13F-POSS-SiH) and hybrid polysiloxane coatings via hydrosilylation.

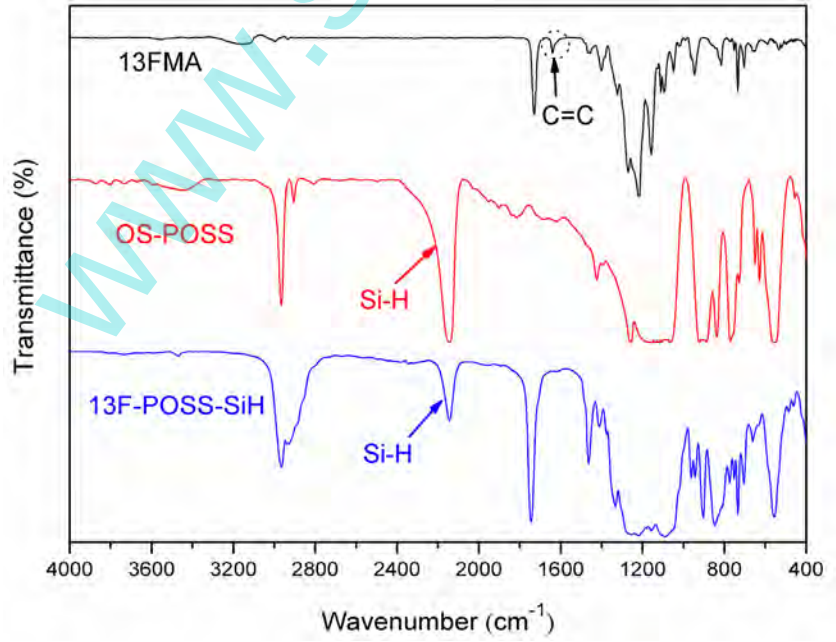

Fig. 1. FTIR spectra of 13FMA, OS-POSS and 13F-POSS-SiH.

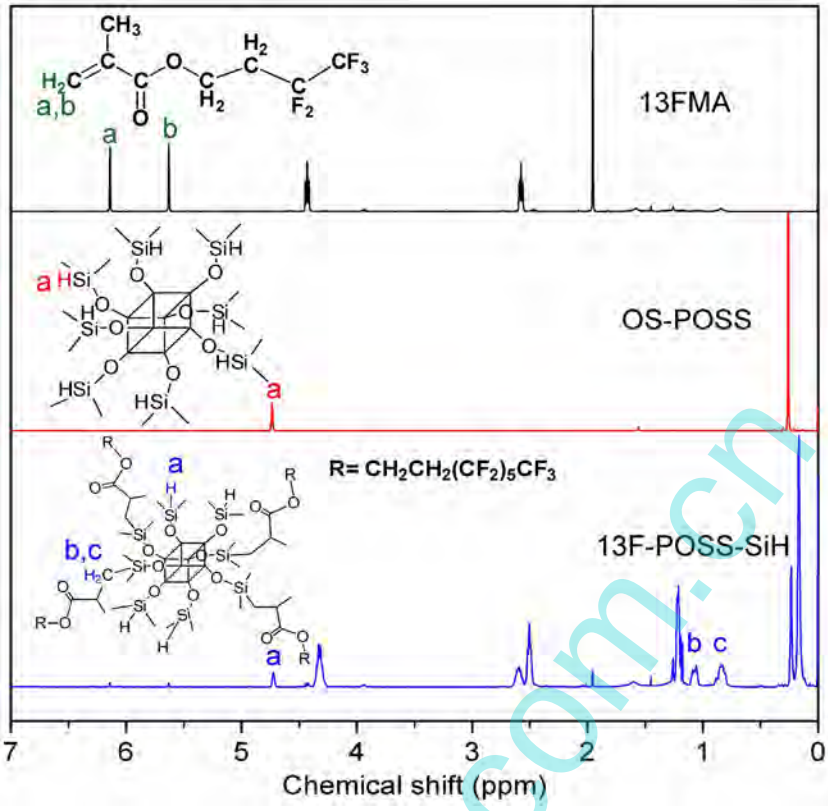

Fig. 2. ^{1}H NMR spectra of 13FMA, OS-POSS and 13F-POSS-SiH.

Table 1
Compositions and surface properties of the hybrid polysiloxane coatings.

Sample[a]	Type of FMA	F-POSS-SiH (wt%)	F-POSS-SiH: PMHS: PMVS (wt/wt/wt)	Height (nm)	Peak interval (μm)	Roughness S_q (nm)	Water contact angle (°)
P10F6	6FMA	10	1: 3.5: 5.5	–	–	–	104.4 ± 0.1
P20F6	6FMA	20	2: 3.5: 4.5	114 ± 18	1.8 ± 0.1	35	104.5 ± 0.3
P30F6	6FMA	30	3: 3.5: 3.5	171 ± 40	2.4 ± 0.3	52	103.7 ± 0.6
P10F12	12FMA	10	1: 3.5: 5.5	177 ± 61	2.0 ± 0.1	60	103.6 ± 0.4
P20F12	12FMA	20	2: 3.5: 4.5	155 ± 43	2.2 ± 0.2	62	103.7 ± 0.2
P30F12	12FMA	30	3: 3.5: 3.5	101 ± 41	2.3 ± 0.2	34	103.8 ± 0.5
P10F13	13FMA	10	1: 3.5: 5.5	526 ± 135	7.3 ± 1.0	188	103.8 ± 0.5
P20F13	13FMA	20	2: 3.5: 4.5	198 ± 23	2.4 ± 0.1	59	103.1 ± 0.6
P30F13	13FMA	30	3: 3.5: 3.5	–	–	–	104.8 ± 0.3
P0	–	–	0: 3.5: 6.5	–	–	–	104.6 ± 0.2

[a] **P*x*** refers to the weight percentage of F-POSS-SiH, and **F*y*** denotes the type of FMA used for preparation of F-POSS-SiH. Sample **P0** without F-POSS-SiH was a control.

AFM images were taken with tapping mode on a CSPM5500A of Being Nano-Instruments Ltd. Guangzhou, China to investigate surface microstructure of the coatings. Water contact angle (WCA), advancing contact angle and receding contact angle were measured at room temperature (25 °C) on a contact angle meter (JC2000D, Shanghai Zhongchen Equipment Ltd., China) equipped with a tilting table with 5 μL water droplets. Contact angle hysteresis (CAH) was defined as the difference between the advancing contact angle and the receding contact angle. Sliding angle (SA) values at room or sub-zero temperatures were also detected with 10 μL water droplets. Each value is the average of 5 independent measurements. The ice shear strength test was conducted on a custom-made device to determine the coating icephobility. The test process has been described in our previous research [43]. Briefly, the Al plate sample (2 cm × 2 cm), on which a hydrophobic hollow cylinder (inner diameter ≈ 1 cm) was placed, was fixed on a cryo-console (STD2-500, Jingie Industry and Trade Co., Tianjin, China). A certain amount of deionized water (450 μL) was pipetted in the cylinder left in a chamber at −15 °C for 2 h to form an ice column. The moving speed of the digital pull&push tester (ZP-500N, Imada, Japan) was 0.5 mm/s. The movement of the tester was commanded by a controller (LSKZA-04, Liansheng Technology Co., Jiangxi, China). The force needed to shear off the ice column was recorded. Each value was recorded by the average of 5 independent measurements. Photos of the coating surfaces were taken immediately after the first ice shear strength test. Moreover, the ice shear strength values of the coatings were recorded for 15 icing/deicing cycles to evaluate the durability of the prepared coatings. According to the reference [48,49], ice accretion tests were performed in a climate chamber (GDW-0100, Nanya Sci-Tech Co., Wuxi, China) with a working temperature at −20 °C (RH: 35%). The coating samples on the Al plate (2 cm × 2 cm) were fixed on a substrate at a tilting angle of 30°. A certain amount of supercooled water (50 g) was then sprayed on the sample in 10 s through a separating funnel pipe at 20 cm overhead. Before spraying supercooled water, samples were placed in the climate chamber for 30 min to ensure them at the measurement

temperature. After spraying, the samples were removed out of the chamber and weighed immediately in an analytical balance. The ice accretion, defined as the increase of the sample mass caused by icing, was calculated from the sample masses before and after the icing process. Each value was recorded by the average of 5 independent measurements. The ice accretion on the bare aluminum plate in the sample size was also measured as a control.

3. Results and discussion

3.1. Characterization of F-POSS-SiH

The products were characterized by FTIR and ^{1}H NMR. Typical FTIR spectra of 13FMA, OS-POSS and 13F-POSS-SiH are shown in Fig. 1. The stretching vibration characteristic peak of vinyl groups at 1600 cm^{-1} is barely discernible in the 13F-POSS-SiH curve, indicating that Pt-catalyzed hydrosilylation was almost finished. Meanwhile, the signal at 2200 cm^{-1}, which belongs to stretching vibration peak of Si-H, indicates there was Si-H left for further crosslinking reaction.

To precisely evaluate the purity of products and calculate the synthesis conversion, ^{1}H NMR analyses were further performed. As shown in Fig. 2 of the ^{1}H NMR spectrum of 13F-POSS-SiH, the appearance of signals at around 0.83 ppm and 1.06 ppm of $-SiMe_2C\underline{H}_2-$ corroborates the successful modification by 13FMA. And, the proton integration ratio of $-C\underline{H}CO-$ around 2.51 ppm and $-$Si-H at 4.70 ppm approached to 1:1, confirming the exact quadri-substitution in 13F-POSS-SiH. ^{1}H NMR characterizations of 6F-POSS-SiH (Fig. S1) and 12F-POSS-SiH (Fig. S2) could be found in the Supplementary data. The proton integration ratio of $-C\underline{H}CO-$ around 2.65 ~ 2.67 ppm and $-$Si-H at 4.72 ppm in the two ^{1}H NMR spectra of F-POSS-SiH approached to 1:1, confirming the quadri-substitution as expected, and suggesting that each F-POSS-SiH molecule has four SiH groups.

3.2. Morphology of the hybrid polysiloxane coatings

The hybrid polysiloxane coatings containing fluorinated POSS were prepared from F-POSS-SiH, PMHS and PMVS with different compositions (Table 1). The thickness of coatings was controlled at around ~230 μm by controlling the solution amount and concentration. Consequently, as shown in SEM images in Fig. 3, obvious micro-sized wavy structure were observed on surfaces of **P20F6**, **P30F6**, **P10F12**, **P20F12**, **P30F12**, **P10F13**, and **P20F13**, but there were no apparently topologic structure on **P10F6** containing a small amount (10 *wt*%) of 6F-POSS-SiH. Typically, similar wavy surfaces could also be observed directly in the OM image of **P20F13** (Fig. 3).

A 40 μm × 40 μm area of each sample with wavy surfaces was also detected in AFM to investigate the micro/nano structure of the wavy topologic surfaces (Fig. 4). Successive protuberances were observed on the samples. To further investigate the size of the successive protuberances, height, peak interval and roughness were analyzed with AFM images by the Imager Software. The protuberance height of **P20F6**, **P30F6**, **P10F12**, **P20F12**, **P30F12**, and **P20F13** ranged from 100 to 200 nm with peak interval from 1.8 to 2.4 μm, roughness S_q from 34 to 62 nm (Table 1). **P10F13** had the roughest surfaces (S_q = 188 nm) with protuberance height of 526 ± 135 nm and peak interval of 7.3 ± 1.0 μm. The shape of the successive protuberances of **P10F13** and **P20F13** was more regular and different from others. No specific topology structure was found on the AFM image of sample **P0** surface, proving F-POSS-SiH was essential for construction of the wavy surface and successive protuberances.

Development of the wavy surfaces was illustrated in Fig. 5(a–d). Three reactants were mixed uniformly in the solution, in which both F-POSS-SiH and PMHS acted as crosslinkers while PMVS as the substrate resin. According to the distribution of the four main elements along the depth of coating sample **P10F13** (Fig. 5(e)), the amount of Si element remained almost the same, while those of C, O, and F elements increased as the scanning position was getting closer to the surface, indicating the migration of fluorinated groups to the top surface. The element contents of C, O, F and Si at six specific spots of the cross-section of sample **P10F13** (Fig. 5(f)) further exemplified the variations. It was suggested that F-POSS-SiH could aggregate to the top of surface through self-assembly at the air/liquid interface driven by the low surface energy of the fluorinated components during the surface dry process and heat treatment, which was confirmed by EDS analysis (Fig. 5(e and f)). Thus, a gradient coating was formed in which F-POSS-SiH was rich on the top layer of the surface, while silicone in the sub-layer of the bulk. Furthermore, the element distribution of the cross-section for sample **P30F6** was also shown in the Supplementary data (Fig. S3) and manifested almost the same variation trend with sample **P10F13**. In addition, it was apparent that sample **P10F13** exhibited more significant contrast in the fluorine content between the surface and the bulk, which could be attributed to the favorable migration of 13F-POSS-SiH.

The agglomeration of F-POSS-SiH and the evaporation of the solvent could induce the volumetric shrinkage of polysiloxane. However, there existed discrepancy between the top and bulk layers. Firstly, F-POSS-SiH mainly accumulated on the top layer, while the bulk layer was mostly composed of polysiloxane, bringing about the rigidity difference between the top and the bulk layers. On the other hand, due to the gradient distribution of F-POSS-SiH, the crosslinking degree varied along the coating depth. Consequently, there was a mismatch in volumetric shrinkage inside the coatings, creating a compressive stress and resultant wavy surfaces, similar to the early report, in which wrinkling morphology patterns were triggered by the migration of fluorinated polyhedral oligomeric silsesquioxanes with thiol groups as a reactive nanoadditive [36].

However, there were not visibly wavy traces on the surface of sample **P10F6**, and obvious phase separation was observed on surface of sample **P30F13** (Fig. 3). It was supposed that the content of different fluorinated components exhibited an influence on the formation of the wavy surfaces. Sufficient contents (20 wt% or 30 wt%) or bigger fluorinated alkyl groups (12FMA or 13FMA) in F-POSS-SiH were necessary. Sample **P10F6** with a relatively lower content of 6F-POSS-SiH (10 wt%) and shorter fluorinated alkyl group (6FMA) could not afford to migration and self-assembly of 6F-POSS-SiH on the surface. Then, a rigid layer on the top of the coating could not form, which in turn could not induce enough compressive stress to generate wavy surfaces. Besides, for sample **P30F13**, excess fluorinated components caused micro-sized phase separation, rather than wavy surfaces [50].

3.3. Wettability of the hybrid polysiloxane coatings

It was reported that the extremely low glass transition temperature of PDMS ensured large free-volume at an ambient temperature, which would act as additional “reservoir” to accommodate the infused silicone oil [24]. In the present system, it was hypothesized that by controlling the dosage, there could be unreacted silicone oil, i.e., PMHS, embedded in the coatings through the crosslinked network and also covered as a lubricating layer. In order to demonstrate free-volume in the coatings for lubricant holding, comparison experiments below were carried out in this study. The coatings without PMHS, labeled as **6F**, **12F** and **13F**, respectively, were prepared from 6F-POSS-SiH, 12F-POSS-SiH or 13F-POSS-SiH with PMVS by ensuring the equivalent molar amount of Si-H in each F-POSS-SiH and C=C in PMVS. Sample **NF** was also prepared from OS-POSS and PMVS as a control. It was found that during the WCA measurement, the water drops gradually sank into the

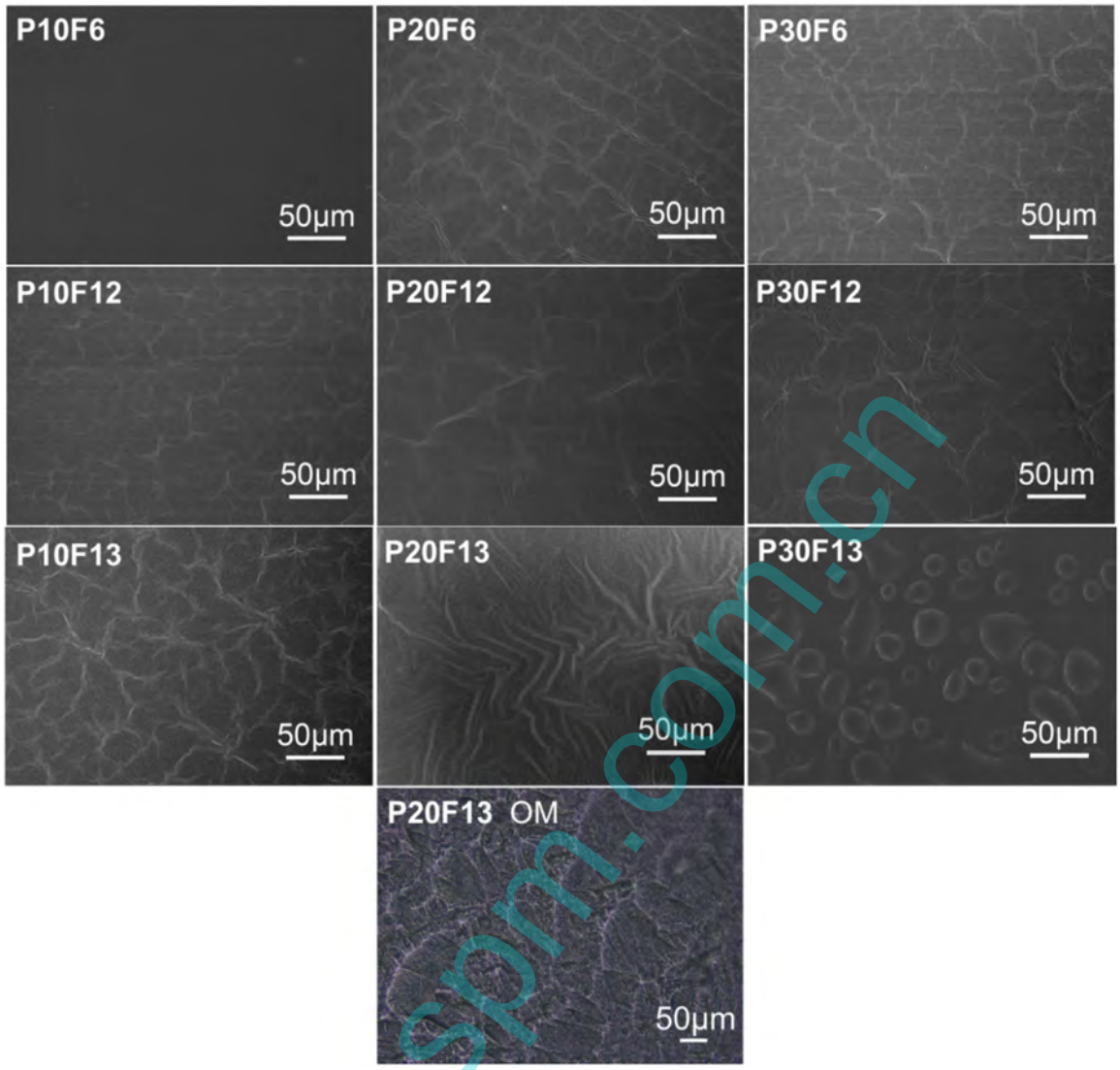

Fig. 3. SEM images of the hybrid polysiloxane surfaces and an OM image of **P20F13**.

films, resulting in the unordinary variation of water contact angle with time. As can be seen in the Supplementary data (Fig. S4), the WCA values of all the four samples decreased sharply in a few seconds, and subsequently reduced slowly after which the WCA values stayed in a constant stage, confirming the free-volume inside the coating. Moreover, when immersed in the compatible silicone oil, PDMS became expanded and readily infused. Further, it was considered that silicone was particularly inclined to infusion due to the low rotational energy barrier around the Me_2Si—O bond (3.3 kJ/mol compared with 13.8 kJ/mol around —CH_2— in polyethylene) that allowed easy diffusion for lubricant throughout the polymer matrix [18]. Therefore, the large free-volume inside the polysiloxane coatings could serve as a "reservoir" to accommodate silicone oil and provided channels for the lubricant to migrate through and out of the coating.

The WCA results of the samples in this work were listed in Table 1. It could be seen that there were no obvious differences between the WCA values (103–104°) of all the samples, and the values were similar to that of **P0** ($104.6 \pm 0.2°$) composed of polysiloxane only without F-POSS-SiH. Therefore, it was indicated that all the hybrid polysiloxane coatings containing F-POSS-SiH were possibly lubricated by silicone oil, i.e., unreacted PMHS.

In the wettability test, the CAH value is a direct indicator of non-sticky property of a solid surface [51]. Furthermore, it was reported that CAH, rather than WCA, is critical for accurately assessing and understanding the resistance to dewetting of liquid drops from solid surfaces [28]. There were also studies coming to a conclusion that a linear correlation between the ice adhesion (which might be governed by work of adhesion) and CAH [52]. In this study, it can be seen from Fig. 6 that the initial CAH values of all the samples were lower than 6°, indicating a 5 μL water droplet could easily slip from the "slippery" surfaces. The CAH value of **P0** is provided for comparison (advancing contact angle $108.3 \pm 0.7°$, receding contact angle $101.8 \pm 0.4°$, CAH $6.5 \pm 0.3°$). The "slippery" surfaces, however, were believed to be resulted from the entrapped lubricating oil and low surface fluorinated components as well as the wavy surface structures. It was supposed that the free-volume inside the coatings and the micro-sized wavy surfaces provided space to accommodate silicone oil, and formed a slippery lubricating layer [24].

Meanwhile, for coatings with the same kind of F-POSS-SiH, there was a downtrend in CAH values as the content of F-POSS-SiH increased (Fig. 6). In consideration of the fixed percentage of PMHS, more PMHS (lubricant) would be remained in the coating without taking part in the crosslinking reaction as the dosage of fluorinated

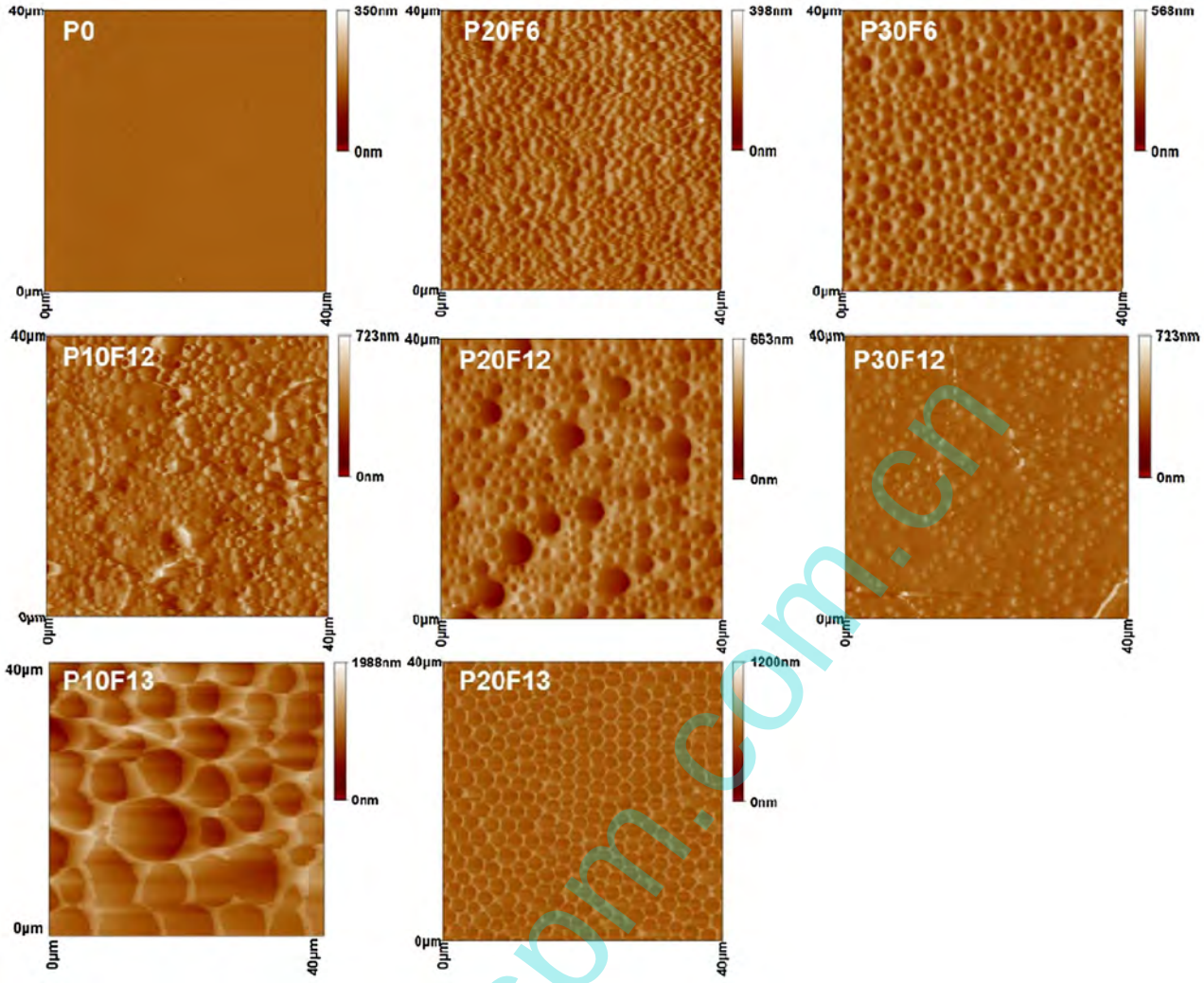

Fig. 4. AFM images of the hybrid polysiloxane coating surfaces.

Table 2
Sliding angle of typical coatings containing 13F-POSS-SiH at different temperatures.

Sample	Sliding angle (°)		
	Room temperature (25 °C)	0 °C	−5 °C
P10F13	3.9 ± 0.2	9.1 ± 0.2	11.0 ± 0.3
P20F13	2.5 ± 0.3	3.5 ± 0.4	4.8 ± 0.3
P30F13	4.7 ± 0.7	6.8 ± 1.6	8.3 ± 0.2

POSS increased, which could be caused by F-POSS-SiH aggregation on the very top of the surface and formation of chemical linkages with PMVS via preferable heating. It was confirmed by a gravimetric analysis. The remaining unreacted PMHS in the coatings was thoroughly dissolved by CH_2Cl_2 and the samples **P10F12**, **P20F12** and **P30F12** were weighed before and after washing the unreacted PMHS. The weight loss of samples **P10F12**, **P20F12** and **P30F12** were 14.3 mg, 14.7 mg and 16.0 mg, respectively. The increase in the fluorine content of F-POSS-SiH would result in lower adhesive force between water and surfaces. Moreover, the depressed affinity between water and surfaces caused by aggregation of 13F-POSS-SiH favored highly slippery properties of the hybrid polysiloxane coatings. The SA values of **P10F13**, **P20F13** and **P30F13** surfaces at room temperature (25 °C), 0 °C and −5 °C were shown in Table 2. Obviously, there was a slight increase in SA values of each sample as the temperature went down. Furthermore, the water droplet moved much slower under 0 °C and −5 °C than it did at room temperature. It was possibly because that water tends to be more viscous at low temperatures. Nevertheless, the water drop could still slide off the surface when tilted at a small angle under subzero temperatures so that supercooling water could not deposit on the coatings. Furthermore, sample **P20F13** exhibited excellent behaviors that could prevent retention of water droplets with SA less than 5° at −5 °C.

3.4. Ice shear strength and ice accretion

Ice shear strength test, which can reveal the adhesion between ice and surfaces, was conducted on the prepared hybrid polysiloxanes as well as Sylgard 184 film and **P0** as controls. The Sylgard 184 films were prepared strictly according to the specification of the purchased product in 10:1 ratio of part A (bulk) and part B (crosslinker). The thickness of the Sylgard 184 was about 200 μm, controlled by a knife coater.

As shown in Fig. 7, ice shear strength values of all the samples except for **P30F13** were lower than 20 kPa, of which the minimum value reached 3.8 ± 1.8 kPa (**P30F12**), about 20 times lower than that of Sylgard 184 (78.0 ± 3.8 kPa). The extreme small value of the ice shear strength was believed to result from the lubricant accommodated in the silicone networks and the micro-sized topologic

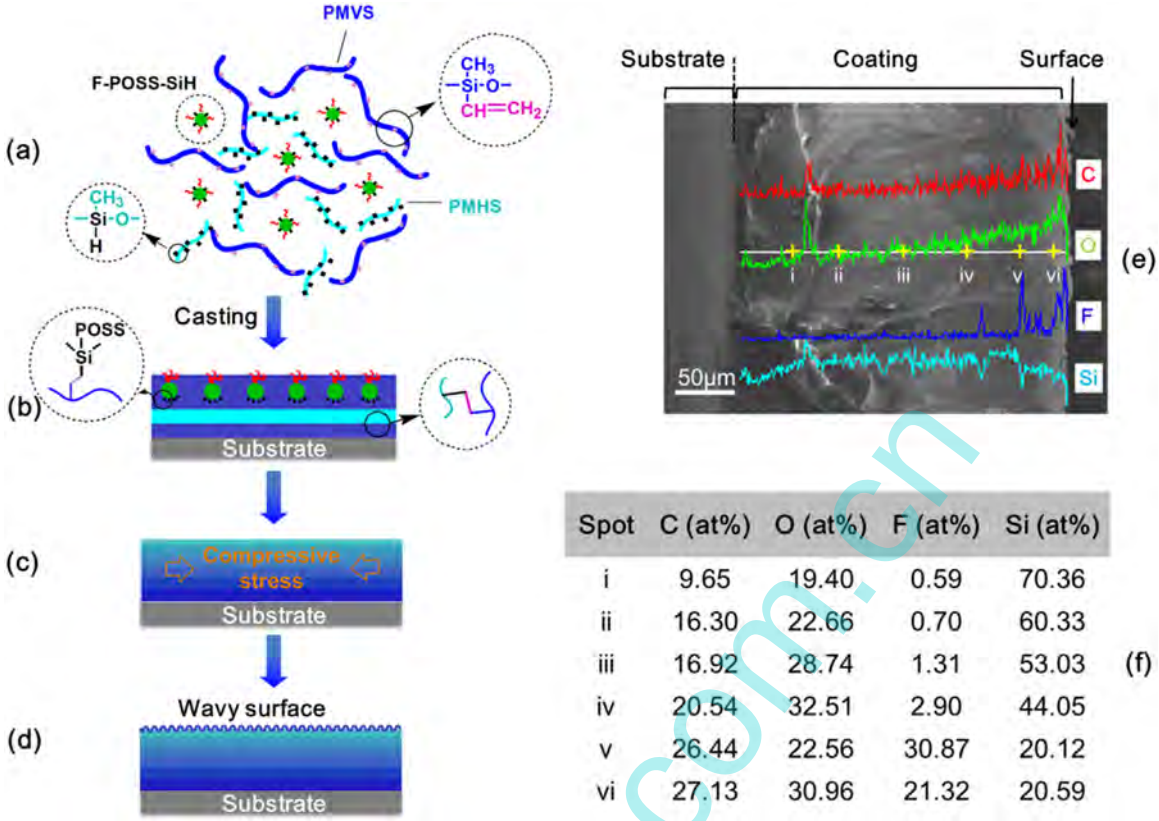

Spot	C (at%)	O (at%)	F (at%)	Si (at%)
i	9.65	19.40	0.59	70.36
ii	16.30	22.66	0.70	60.33
iii	16.92	28.74	1.31	53.03
iv	20.54	32.51	2.90	44.05
v	26.44	22.56	30.87	20.12
vi	27.13	30.96	21.32	20.59

(f)

Fig. 5. Schematic illustration of formation of the slippery wavy surfaces. (a) Reaction of F-POSS-SiH, PMVS and PMHS; (b) coating formation and self-aggregation of F-POSS-SiH; (c) generation of compressive stress on the surface of coating; (d) formation of wavy surfaces; (e) EDS spectra of the cross section of sample **P10F13**, and there appears an obvious accumulation of C, O, and F on the surface; (f) element contents of **P10F13** at corresponding spots as shown in (e).

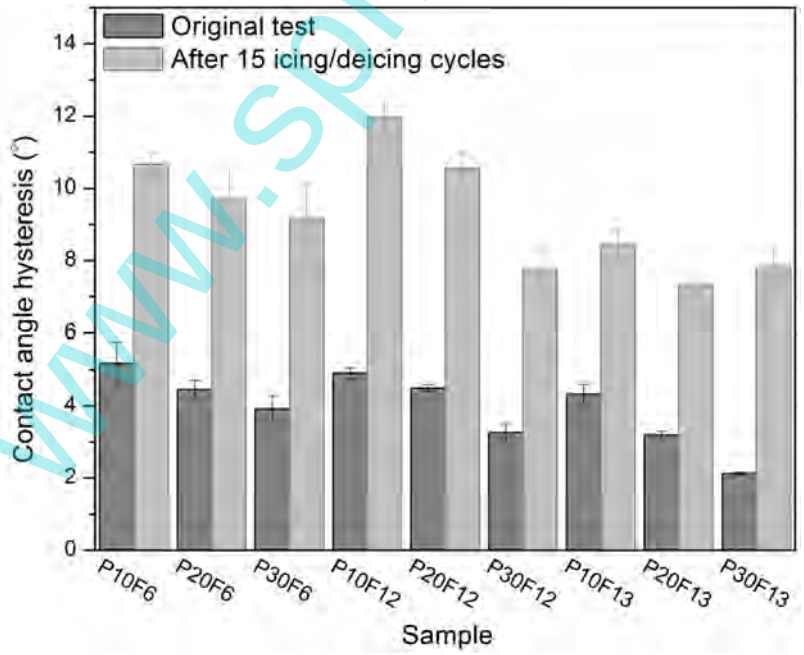

Fig. 6. Comparison of the water contact angle hysteresis (CAH) values of the hybrid polysiloxane coatings before (Original test) and after 15 icing/deicing cycles.

surfaces generated by the self-aggregation of low surface energy fluorinated POSS as well. Meanwhile, sample **P0** exhibited ice shear strength of 42.9 ± 7.4 kPa. It could be caused by the absence of the low surface energy FMA component and its flat surface which could hardly retain lubricating oil. Wang et al. developed silicone-oil-infused PDMS coatings with different silicone oil contents and did comparatively overall researches on wettability and anti-icing property which showed quite promising results [24]. By comparison, in this work, all the above features made the prepared slippery

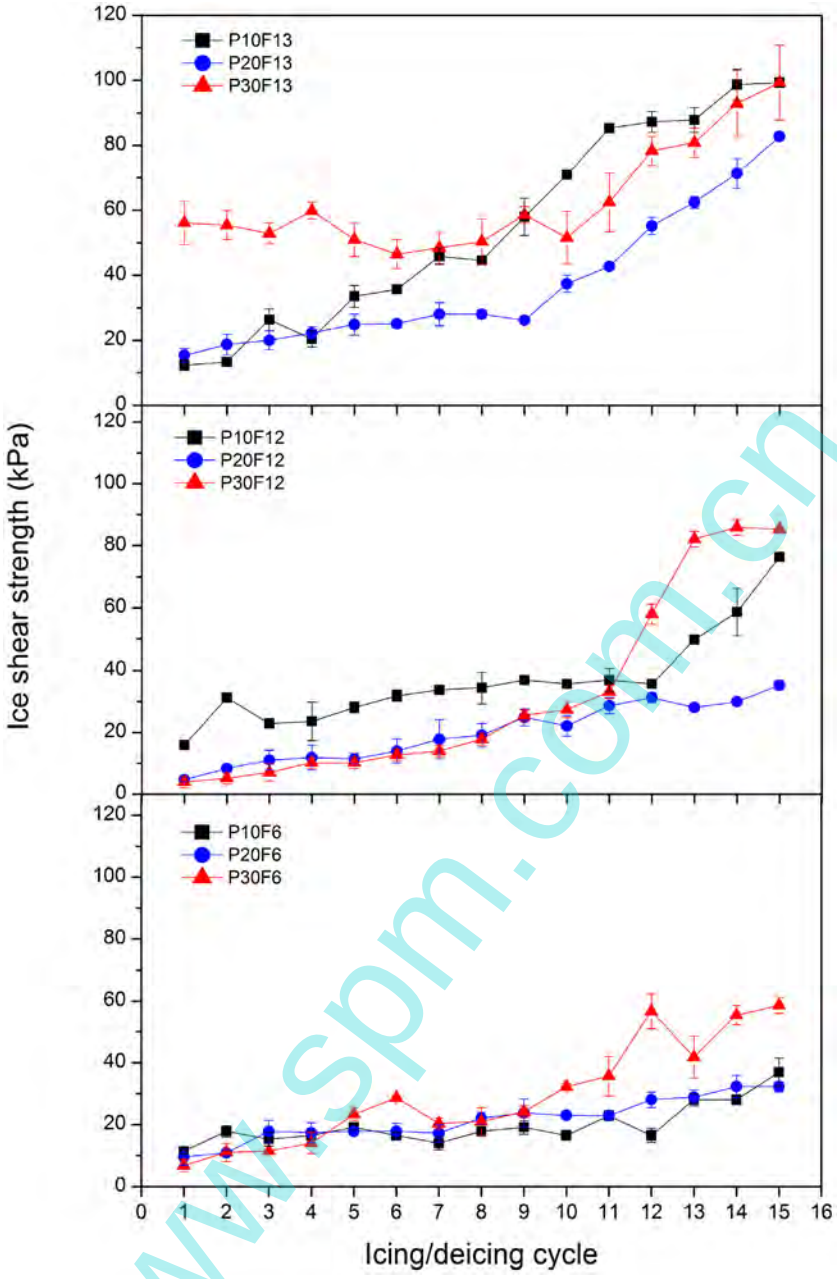

Fig. 7. Variations of the ice shear strength of the hybrid polysiloxane coatings during icing/deicing tests.

polysiloxane coatings with small CAH and low ice shear strength values effective for icephobicity.

Although **P30F13** sample possesses lower affinity with water, its ice shear strength increased to 56.1 ± 6.6 kPa, the maximum value in the system. It might be caused by the obvious phase separation appeared on **P30F13** surface (Fig. 3). Irregular circle slices of tens to hundreds micrometers instead of wavy surfaces were observed in the SEM image. According to topological imaging contrast in SEM, it was demonstrated that the irregular slices on the surface cocked up from edges (lighter margin). Consequently, lubricating oil could not be accommodated and locked on the surfaces. In addition, it was supposed that highly roughed surfaces were fully wetted, and thus when the water freezes, ice was embedded and stronger bonding between ice with the coating formed because of the mechanical interlocking effect, leading to higher adhesion strength [3]. The cocking up slices in the **P30F13** sample brought roughness of hundreds of micrometers, leaving large space for ice formation and making it difficult for the coating to be deiced.

Furthermore, it was reported that the residual ice crystals left after the adhesion test would reflect the adhesion between ice and surface. The small amount of residual ice crystals indicated a loose ice structure at the interface between the ice block and the substrate [53]. In this study, the residual ice crystals shown in the Supplementary data (Fig. S5) demonstrate that the ice column left the surface without splitting inside, suggesting that there was no interlocking effect between ice and surface.

Ice accretion tests were carried out to further illustrate the coatings' icephobic properties. As shown in Fig. 8, ice accretion values of all the samples containing F-POSS-SiH were below 20% in comparison with bare aluminum, e.g., 1.2 ± 0.6 mg of **P20F13,** 39.8 ± 3.6 mg of **P0** for comparison and 59.5 ± 5.5 mg of bare aluminum as control, confirming the surfaces remain slippery under supercooled conditions.

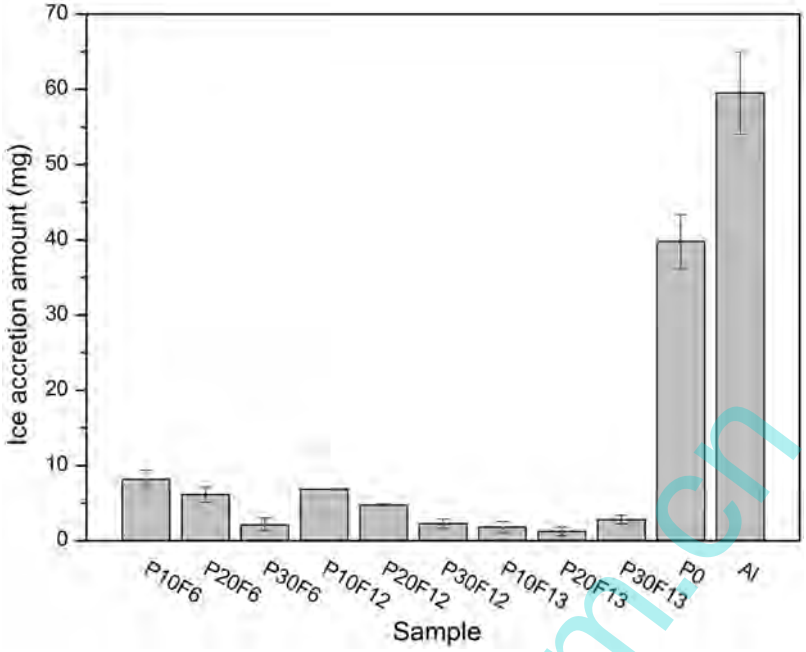

Fig. 8. Ice accretion of the hybrid polysiloxane coatings in comparison with **P0** and Al.

Furthermore, photos recording the surface of **P30F12** and bare aluminum after ice accretion tests (Supplementary data, Fig. S6) directly reflect the difference between the hybrid polysiloxane coatings with lubricant and bare aluminum.

3.5. Durability of the hybrid polysiloxane coatings

Since the lubricant was one of the principal factors that contributed to the slippery icephobic properties, the durability of the sacrificial coatings should be taken into consideration. We conducted icing/deicing cycles of the ice shear strength test on each sample, and investigated the changes of CAH and morphology after 15 cycle tests.

Changes of the ice shear strength with the number of icing/deicing cycles were shown in Fig. 7. It could be seen that, with the increased number of icing/deicing cycle, the ice shear strength of the coatings exhibited a gradual increase tendency due to the consumption of the lubricant silicone oil. The phenomenon was also found in the self-lubricating water layer for anti-icing [19]. However, even after 15 icing/deicing cycles, the ice shear strength values of the prepared coatings were still less than 100 kPa, much lower than that of bare aluminum (1417 ± 139 kPa), suggesting the coatings still exhibited icephobic properties. For example, the **P20F12** sample still exhibited a very low ice shear strength value at 35.2 ± 1.6 kPa. The results demonstrate the notion of maintaining the slippery property via self-replenishment from inside the silicone network where the lubricant could be stored.

Comparison between CAH at the beginning and after the 15th cycle was shown in Fig. 6. CAH of each sample increased obviously by several degrees ranging from 4° to 8°. However, all values after the 15th cycle were still lower than 13° (i.e., sample **P20F13** still exhibited CAH of 7.3 ± 0.2°), confirming the micro-sized roughness and low surface energy fluorinated components on the very top layer contribute to the wettability and icephobic properties.

Furthermore, we tried to figure out the deicing mechanism on analysis of the shear stress-displacement curves. As seen in Fig. 9, obvious distinctions between curves during the 1st and 15th tests were detected. As for the surface with lubricant at the beginning of the 1st test, the shear stress increased to the maximum till the

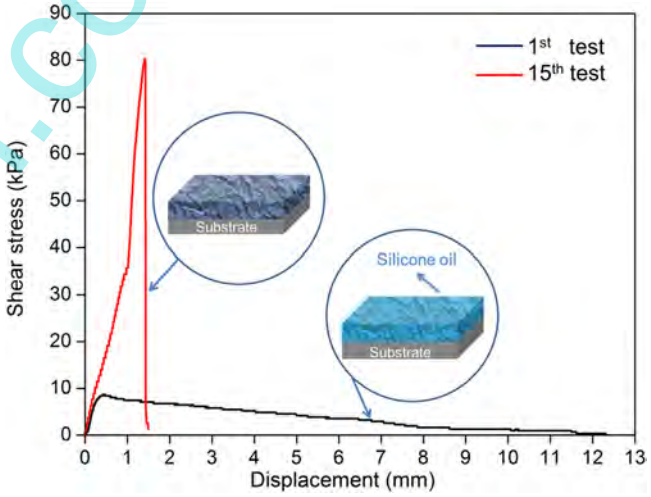

Fig. 9. Typical shear stress-displacement curves of sample **P30F12** during the 1st and 15th tests. Insets indicated the lubricant was drained off during the test. The displacement was defined as the moving length of the ice column when pushed.

ice shear strength value in a very short displacement, after which the value slowly reduced to zero. It was assumed that the static friction force between the slippery surface and ice column could easily rise to the highest. Afterward, the force became sliding friction, while value depended on the surface properties and vertical stress. However, the retardation of viscous silicone oil and the varied friction coefficient induced by diverse roughness would cause variation of sliding friction during the removal of the ice column off the surfaces. On the contrary during the 15th test, it took several seconds for the shear stress to climb to the peak (ice shear strength value), followed by a sharp decrease to zero. This demonstrates that the silicone oil was sacrificing and the surfaces tended to become smoother during the icing/deicing cycles. Furthermore, a great disparity apparently existed between ice shear strength values of the 1st and 15th tests in Fig. 6 (8.4 kPa and 80.3 kPa). Furthermore, systematical study of the deicing mechanism would help make out the lubrication behaviors and the service life of the coatings.

4. Conclusions

An efficacious and durable icephobic coating based on polysiloxane was developed through hydrosilylation of PMVS, PMHS and fluorinated POSS containing −SiH groups as well. Three kinds of F-POSS-SiH, i.e., 6F-POSS-SiH, 12F-POSS-SiH and 13F-POSS-SiH, were synthesized and introduced into the icephobic system to generate the micro-sized wavy surfaces, on which or in the coatings PMHS as a lubricant existed. All the prepared hybrid polysiloxane coatings were proved to be slippery with CAH values lower than 10°. Moreover, the CAH value decreased with increase of the F-POSS-SiH content by using the same kind of F-POSS-SiH. The slippery hybrid coatings containing F-POSS-SiH exhibited extremely low ice shear strength. Among them, the minimum value of **P30F12** reached 3.8 ± 1.8 kPa, and its ice shear strength remained below 100 kPa after 15 icing/deicing cycles. Specifically, some of them still had lower ice shear strengths than 40 kPa, such as **P20F12** with 35.2 ± 1.6 kPa at the 15^{th} test. The slippery coatings composed of polysiloxane and fluorinated POSS exhibited extraordinarily high icephobicity, showing their potential application as icephobic coatings.

Acknowledgments

This work is sponsored by National Natural Science Foundation of China (No. 51273146) and Natural Science Foundation of Tianjin, China (No. 14ZCZDGX00008).

Appendix A. Supplementary data

Supplementary data associated with this article can be found, in the online version, at http://dx.doi.org/10.1016/j.porgcoat.2016.11.018.

References

[1] A.G. Kraj, E.L. Bibeau, Phases of icing on wind turbine blades characterized by ice accumulation, Renew. Energy 35 (2010) 966–972.
[2] Y. He, C. Jiang, P. Hu, R. Yang, W. Tian, W. Yuan, Reducing ice accumulation and adhesion by using a flexible micro-rod film, Cold Reg. Sci. Technol. 118 (2015) 57–63.
[3] S.A. Kulinich, S. Farhadi, K. Nose, X.W. Du, Superhydrophobic surfaces: are they really ice-repellent, Langmuir 27 (2011) 25–29.
[4] F. Tavakoli, H.P. Kavehpour, Cold-induced spreading of water drops on hydrophobic surfaces, Langmuir 31 (2015) 2120–2126.
[5] X.X. Zhang, M. Chen, M. Fu, Impact of surface nanostructure on ice nucleation, J. Chem. Phys. 141 (2014) 124709.
[6] P. Tourkine, M. Le Merrer, D. Quéré, Delayed freezing on water repellent materials, Langmuir 25 (2009) 7214–7216.
[7] D. Richard, C. Clanet, D. Quéré, Surface phenomena: contact time of a bouncing drop, Nature 417 (2002), 811–811.
[8] C. Clanet, C. Béguin, D. Quéré, D. Richard, Maximal deformation of an impacting drop, J. Fluid Mech. 517 (2004) 199–208.
[9] S. Zheng, C. Li, Q. Fu, W. Hu, T. Xiang, Q. Wang, M.P. Du, X.C. Liu, Z. Chen, Development of stable superhydrophobic coatings on aluminum surface for corrosion-resistant self-cleaning, and anti-icing applications, Mater. Des. 93 (2016) 261–270.
[10] J.H. Li, Q. Liu, Y.L. Wang, R.R. Chen, K. Takahashi, R.M. Li, L.H. Liu, J. Wang, Formation of a corrosion-resistant and anti-icing superhydrophobic surface on magnesium alloy via a single-step method, J. Electrochem. Soc. 163 (2016) 213–220.
[11] Y. Shen, J. Tao, H. Tao, S. Chen, L. Pan, T. Wang, Anti-icing potential of superhydrophobic Ti6Al4 V surfaces: ice nucleation and growth, Langmuir 31 (2015) 10799–10806.
[12] A.J. Meuler, G.H. McKinley, R.E. Cohen, Exploiting topographical texture to impart icephobicity, ACS Nano 4 (2010) 7048–7052.
[13] J. Chen, J. Liu, M. He, K.Y. Li, D.P. Cui, Q.L. Zhang, X.P. Zeng, Y.F. Zhang, J.J. Wang, Y.L. Song, Superhydrophobic surfaces cannot reduce ice adhesion, Appl. Phys. Lett. 101 (2012) 111603.
[14] K.K. Varanasi, T. Deng, J.D. Smith, M. Hsu, N. Bhate, Frost formation and ice adhesion on superhydrophobic surfaces, Appl. Phys. Lett. 97 (2010) 234102.
[15] P.W. Wilson, W. Lu, H. Xu, P. Kim, M.J. Kreder, J. Alvarenga, J. Aizenberg, Inhibition of ice nucleation by slippery liquid-infused porous surfaces (SLIPS), Phys. Chem. Chem. Phys. 15 (2013) 581–585.
[16] S.B. Subramanyam, K. Rykaczewski, K.K. Varanasi, Ice adhesion on lubricant-impregnated textured surfaces, Langmuir 29 (2013) 13414–13418.
[17] R. Dou, J. Chen, Y.F. Zhang, X.P. Wang, D.P. Cui, Y.L. Song, L. Jiang, J.J. Wang, Anti-icing coating with an aqueous lubricating layer, ACS Appl. Mater. Interfaces 6 (2014) 6998–7003.
[18] J. Chen, Z.Q. Luo, Q.R. Fan, J.Y. Lv, J.J. Wang, Anti-ice coating inspired by ice skating, Small 10 (2014) 4693–4699.
[19] J. Chen, R.M. Dou, D.P. Cui, Q.L. Zhang, Y.F. Zhang, F.J. Xu, X. Zhou, J.J. Wang, Y.L. Song, L. Jiang, Robust prototypical anti-icing coatings with a self-lubricating liquid water layer between ice and substrate, ACS Appl. Mater. Interfaces 5 (2013) 4026–4030.
[20] S. Ozbay, C. Yuceel, H.Y. Erbil, Improved icephobic properties on surfaces with a hydrophilic lubricating liquid, ACS. Appl. Mater. Interfaces 7 (2015) 22067–22077.
[21] F.T. Liu, Q.M. Pan, Facile fabrication of robust icephobic polyurethane sponges, Adv. Mater. Interfaces 2 (2015) 1500219.
[22] J.S. Zigmond, K.A. Pollack, S. Smedley, J.E. Raymond, L.A. Link, A. Pavía-Sanders, M. Hickner, K.L. Wooley, Investigation of intricate, amphiphilic crosslinked hyperbranched fluoropolymers as anti-icing coatings for extreme environments, J. Polym. Sci. Polym. Chem. 54 (2016) 238–244.
[23] S. Chernyy, M. Järn, K. Shimizu, A. Swerin, S.U. Pedersen, K. Daasbjerg, L. Makkonen, P. Claesson, J. Iruthayaraj, Superhydrophilic polyelectrolyte brush layers with imparted anti-icing properties: effect of counter ions, ACS Appl. Mater. Interfaces 6 (2014) 6487–6496.
[24] L. Zhu, J. Xue, Y.Y. Wang, Q.M. Chen, J.F. Ding, Q.J. Wang, Ice-phobic coatings based on silicon-oil-infused polydimethylsiloxane, ACS Appl. Mater. Interfaces 5 (2013) 4053–4062.
[25] Q. Liu, Y. Yang, M. Huang, Y.X. Zhou, Y.Y. Liu, X.D. Liang, Durability of a lubricant-infused electrospray silicon rubber surface as an anti-icing coating, Appl. Surf. Sci. 346 (2015) 68–76.
[26] M. Watanabe, R. Hashimoto, Area-selective microwrinkle formation on poly(dimethylsiloxane) by treatment with strong acid, J. Polym. Sci. Polym. Phys. 53 (2015) 167–174.
[27] L.J.T. Landherr, C. Cohen, P. Agarwal, L.A. Archer, Interfacial friction and adhesion of polymer brushes, Langmuir 27 (2011) 9387–9395.
[28] D.F. Cheng, C. Urata, B. Masheder, A. Hozumi, A physical approach to specifically improve the mobility of alkane liquid drops, J. Am. Chem. Soc. 134 (2012) 10191–10199.
[29] L.M. Wang, T.J. McCarthy, Covalently attached liquids: instant omniphobic surfaces with unprecedented repellency, Angew. Chem. Int. Ed. 55 (2016) 244–248.
[30] C. Yang, F.J. Wang, W. Li, J.F. Ou, C.Q. Li, A. Amirfazli, Anti-icing properties of superhydrophobic ZnO/PDMS composite coating, Appl. Phys. A Mater. 122 (2016) 1–10.
[31] M.J. Kreder, J. Alvarenga, P. Kim, J. Aizenberg, Design of anti-icing surfaces: smooth, textured or slippery? Nat. Rev. Mater. 1 (2016) 15003.
[32] T. Deng, K.K. Varanasi, M. Hsu, N. Bhate, C. Keimel, J. Stein, M. Blohm, Nonwetting of impinging droplets on textured surfaces, Appl. Phys. Lett. 94 (2009) 133109.
[33] J.Y. Lv, Y.L. Song, L. Jiang, J.J. Wang, Bio-inspired strategies for anti-icing, ACS Nano 8 (2014) 3152–3169.
[34] X.M. Chen, R.Y. Ma, H.B. Zhou, X.F. Zhou, L.F. Che, S.H. Yao, Z.K. Wang, Activating the microscale edge effect in a hierarchical surface for frosting suppression and defrosting promotion, Sci. Rep. U.K. 3 (2013) 1–8.
[35] J.L. Yagüe, J. Yin, M.C. Boyce, K.K. Gleason, Design of ordered wrinkled patterns with dynamically tuned properties, Phys. Procedia 46 (2013) 40–45.
[36] Y.C. Gan, X.S. Jiang, J. Yin, Self-wrinkling patterned surface of photocuring coating induced by the fluorinated POSS containing thiol groups (F-POSS-SH) as the reactive nanoadditive, Macromolecules 45 (2012) 7520–7526.
[37] W. Ding, Y. Yang, Y. Zhao, S.C. Jiang, Y.P. Cao, C.H. Lu, Well-defined orthogonal surface wrinkles directed by the wrinkled boundary, Soft Matter 9 (2013) 3720–3726.
[38] K. Golovin, D.H. Lee, J.M. Mabry, A. Tuteja, Transparent flexible, superomniphobic surfaces with ultra-low contact angle hysteresis, Angew. Chem. Int. Ed. 52 (2013) 13007–13011.
[39] H. Dodiuk, S. Kenig, A. Dotan, Do self-cleaning surfaces repel ice? J. Adhes. Sci. Technol. 26 (2012) 701–714.
[40] H.X. Wang, Y.H. Xue, J. Ding, L.F. Feng, X.G. Wang, T. Lin, Durable, self-healing superhydrophobic and superoleophobic surfaces from fluorinated-decyl polyhedral oligomeric silsesquioxane and hydrolyzed fluorinated alkyl silane, Angew. Chem. Int. Ed. 50 (2011) 11433–11436.
[41] K. Tanaka, Y. Chujo, Advanced functional materials based on polyhedral oligomeric silsesquioxane (POSS), J. Mater. Chem. 22 (2012) 1733–1746.
[42] D.B. Cordes, P.D. Lickiss, F. Rataboul, Recent developments in the chemistry of cubic polyhedral oligosilsesquioxanes, Chem. Rev. 110 (2010) 2081–2173.
[43] X.H. Li, K.Q. Zhang, Y.H. Zhao, K.Y. Zhu, X.Y. Yuan, Enhancement of icephobic properties based on UV-curable fluorosilicone copolymer films, RSC Adv. 110 (2015) 90578–90587.
[44] X.H. Li, Y.H. Zhao, H. Li, X.Y. Yuan, Preparation and icephobic properties of polymethyltrifluoropropylsiloxane-polyacrylate block copolymers, Appl. Surf. Sci. 316 (2014) 222–231.
[45] K.Q. Zhang, J.Z. Cai, X.H. Li, H. Li, Balance of polyacrylate-fluorosilicone block copolymers as icephobic coatings, Chin. J. Polym. Sci. 33 (2015) 153–162.
[46] H. Li, X.H. Li, C.H. Luo, Y.H. Zhao, X.Y. Yuan, Icephobicity of polydimethylsiloxane-*b*-poly(fluorinated acrylate), Thin Solid Films 573 (2014) 67–73.

[47] Y.C. Li, C. Luo, X.H. Li, K.Q. Zhang, Y.H. Zhao, K.Y. Zhu, X.Y. Yuan, Submicron/nano-structured icephobic surfaces made from fluorinated polymethylsiloxane and octavinyl-POSS, Appl. Surf. Sci. 360 (2016) 113–120.
[48] Z.Q. Yuan, J.P. Bin, X. Wang, Q.L. Liu, D.J. Zhao, H. Chen, H.Y. Jiang, Preparation and anti-icing property of a lotus-leaf-like superhydrophobic low-density polyethylene coating with low sliding angle, Polym. Eng. Sci. 52 (2012) 2310–2315.
[49] S. Ozbay, H.Y. Erbil, Ice accretion by spraying supercooled droplets is not dependent on wettability and surface free energy of substrates, Colloid Surf. A 5 (2016) 210–218.
[50] X. Ye, B. Zuo, M. Deng, Y. Hei, H. Ni, X. Lu, X. Wang, Surface segregation of fluorinated moieties on poly(methyl methacrylate-ran-2-perfluorooctylethyl methacrylate) films during film formation: entropic or enthalpic influences, J. Colloid Interface Sci. 349 (2010) 205–214.
[51] F. Li, F. Mugele, How to make sticky surfaces slippery: contact angle hysteresis in electrowetting with alternating voltage, Appl. Phys. Lett. 92 (2008) 244108.
[52] Y. He, C.Y. Jiang, X.B. Cao, Reducing ice adhesion by hierarchical micro-nano-pillars, Appl. Surf. Sci. 305 (2014) 589–595.
[53] Q.T. Fu, X.H. Wu, D. Kumar, J.W.C. Ho, P.D. Kanhere, N. Srikanth, E. Liu, P. Wilson, Z. Chen, Development of sol-gel icephobic coatings: effect of surface roughness and surface energy, ACS Appl. Mater. Interfaces 6 (2014) 20685–20692.